

**OBSERVATIONS INDICATING THAT $\sim 1 \times 10^7$ K SOLAR FLARE PLASMAS MAY
BE PRODUCED IN SITU FROM $\sim 1 \times 10^6$ K CORONAL PLASMA**

by

U. Feldman^{1,2}, I. Dammasch³, E. Landi^{1,2}, and G. A. Doschek²

March 8, 2004

Submitted to the *Astrophysical Journal*

¹ Artep Inc., 2922 Excelsior Springs, Ellicott City, MD 21042, USA

² E. O. Hulburt Center for Space Research, Naval Research Laboratory, Washington DC
20375-5320, USA

³ Mullard Space Science Laboratory, Holmbury St Mary, Dorking, Surrey RH5 6NT, UK

ABSTRACT

We discuss a set of flare observations obtained at a position of $0.10 R_{\odot}$ above the solar north-west limb. The data were acquired by the Solar Ultraviolet Measurements of Emitted Radiation (SUMER) spectrometer on the *Solar and Heliospheric Observatory* (*SOHO*). We derive time dependent comparisons of physical properties, such as electron temperature and density, between flare plasma and background coronal plasma observed along the same lines-of-sight. In addition to temperature and density, we discuss emission measures, elemental abundances, non-thermal mass motions (from line widths) and bulk mass motions (from Doppler shifts). The observations appear to indicate that the flaring plasmas ($4 \times 10^6 \leq T_e \leq 1 \times 10^7$ K) along the lines-of-sight were formed by in situ heating and possibly by compression of the ambient coronal material ($T_e \leq 2 \times 10^6$ K).

Subject headings: Sun: flares- Sun: corona- Sun: UV radiations

1. INTRODUCTION

The physical mechanisms that produce high-density plasmas in solar flares at temperatures in the 10^7 K range are a subject of intense research. Simulations of electron beam models predict scenarios where 10^7 K flaring plasmas are produced by energetic particles generated in the corona that propagate along magnetic field lines towards the chromosphere where they collide with the local material, and heat and “evaporate” it at speeds of $\sim 200\text{--}800$ km s⁻¹ into coronal loops (e.g., Li, Emslie, & Mariska 1989, Doschek et al. 1986). To date there is no unequivocal observational evidence that all of the high temperature plasmas populating flaring loops is “evaporated” from the chromosphere, either by electron beams or conduction fronts. Also, there are quantitative difficulties in reconciling 1D model predictions of high speed upflows with high speed upflow observations (e.g., see Mariska, Doschek, & Bentley 1993 for a discussion of the observations). For example, in analyzing high spectral resolution X-ray data from intense flares, observed by SOLFLEX on the Air Force *P78-1* satellite, Feldman et al. (1980) and Doschek et al. (1980) found that the highest velocities present in flares occurred during the rise phases and that they did not appear to contain sufficient emission measure to supply all of the required amount of high temperature plasma. Earlier Feldman, Doschek, & Kreplin (1980) postulated that the 10^7 K flare plasma was ambient low-density coronal plasma that was compressed by several orders of magnitude and heated from the $\sim 1 \times 10^6$ K range to the $\sim 1 \times 10^7$ K range. Not envisioning any compression mechanism other than by azimuthal magnetic fields, they postulated that high temperature plasma may result from sudden discharges of electric currents along coronal loops causing the plasmas trapped in them to

compress and heat. Much earlier Alfvén & Carlqvist (1967) introduced a flare model based on current interruption in twisted magnetic ropes.

Another argument against a pure evaporation picture concerns elemental abundances. Although elemental abundances in the chromosphere have in some cases been found to be enhanced relative to those in the photosphere (Feldman, Widing, & Lund 1990, Athay 1994), elemental abundances of coronal plasmas above active regions are in some instances very different from those in the photosphere. Therefore they can be used as tracers when attempting to identify sources of flaring plasmas that occur within these active regions. Studies of coronal active regions and the flares occurring in them show that the plasmas in both have similar coronal elemental abundances, although from composition studies alone the exact source of the flaring material could not be pinpointed (for details see McKenzie & Feldman 1992; Feldman 1996, and Feldman & Laming 2000).

We believe that we have found a set of observations that may indicate that at least some flaring plasmas ($4 \times 10^6 \leq T_e \leq 1 \times 10^7$ K) are formed by in situ heating, possibly produced by compression of ambient coronal plasmas ($T_e \leq 2 \times 10^6$ K). The evidence is based on a sequence of high spatial and spectral resolution spectra from which electron temperatures, densities, emission measures, elemental abundances, and mass motions can be derived. The spectra were acquired by the Solar Ultraviolet Measurements of Emitted Radiation (SUMER) spectrometer on the *Solar and Heliospheric Observatory (SOHO)* spacecraft during a flare watch campaign. The observations are described in Section 2, physical properties of the observed flaring and coronal plasmas derived from the observations are described in Section 3, and a summary and discussion of the results are given in Section 4.

2. OBSERVATIONS

The observations discussed in this paper concern a number of flares that erupted above the north-west limb over 38 hours between 14:30 UT, April 23 and 04:30 UT, April 25, 2003. The flares occurred in NOAA region 10339 that was listed in the Solar Geophysical Data Comprehensive Reports for April 20, about 4 days prior to the observations. Using full Sun images recorded by the Michelson Doppler Imager (MDI) on *SOHO* (Scherrer et al. 1995), we were able to track the active region producing the flares back to the time it appeared on the east limb, concluding that it was at least two weeks old. The Fe XII 195 Å channel images recorded by the Extreme-Ultraviolet Imaging Telescope (EIT) on *SOHO* (Delaboudinière 1995) also support this conclusion. In addition, the main coronal features of the region, as seen in the Fe XII images, are two pairs of spike-like diverging emission structures extending upward and outward from a base at a lower altitude. Widing & Feldman (1989, 1993) noted that such diverging structures are one of the main characteristics of single solar regions with unusually large abundance enrichments (~ 10) of elements having first ionization potentials (FIP) < 10 eV. (Coronal elemental enrichments are defined as ratios of coronal abundances to photospheric abundances).

2.1 X-ray Observations

X-ray data records from the 12th *Geostationary Environmental Satellite (GOES-12)* show (Figure 1) that during the 38 hour observations, 4 medium size flares (X-ray class $\geq C2$, i.e., $\geq 2 \times 10^{-6}$ watt m⁻²) and a number of smaller ones erupted on the Sun. The X-ray background as measured by the 1-8 Å detector was at the time between $4-5 \times 10^{-7}$ watt m⁻²,

i.e., between B4 and B5. Columns 1 and 2 of Table 1 list onset times and *GOES* classes of flares of X-ray class $\geq C2$ present on the *GOES* recordings. The table also lists information regarding a B8 flare that erupted at $\sim 21:30$ UT April 23 to be discussed later. Column 5 of Table 1 lists the coordinates of the *GOES* flares as determined from ground-based $H\alpha$ flare patrol observations. Flares erupting on the disk are usually observed by ground-based observatories but those occurring at the limb are in many cases not detected. According to $H\alpha$ records published by the Solar Geographical Data Prompt Reports, the M3 flare that erupted at 12:50 UT on April 24 occurred on the disk, and so it will not be discussed any further. Also the X-ray flux of the flare that erupted at $\sim 05:30$ UT April 24 and was reported as C5 was due to two flares that erupted nearly simultaneously, one on the disk and observed by ground-based flare patrol telescopes, and a second that occurred above the west limb and was recorded by SUMER. A discussion of SUMER flares will be given later.

2.2 SUMER Flare Observations

The SUMER instrument (Wilhelm et al. 1995) on *SOHO* is a normal incidence high spectral ($\delta\lambda \sim 0.043 \text{ \AA}$ in 1st order) and spatial resolution ($\delta\phi = 1''$) slit spectrometer. Its 1024x360 pixel detector is designed to record spectra in a 43 \AA wide section in 1st order. The recorded information on the entire detector or any part of it is transmitted to ground stations. The cadences at which images are transmitted depend on the number of transmitted pixels. During the observations considered in the present work, the transmitted data were limited to three wavelength ranges, each 50x360 pixel ($\sim 2 \text{ \AA}$) wide, resulting in a transfer rate of one image per 49.5 s. For each of the observations one wavelength window was centered on an

Fe XIX line. Two other windows were centered either on Ca X and Si III lines, or alternatively on Fe XVII and Ca XIII lines. The lines, their spectroscopic identifications, and the temperatures at which their fractional ion abundances are at a maximum in ionization equilibrium, are listed in Table 2 for the two sequences. The emissivity curves of the iron and calcium lines in Table 2, to be discussed in the following section, have been calculated using the CHIANTI database (Dere et al. 2001, Young et al. 2003), the Mazzotta et al. (1998) ion fraction tables, and the Grevesse & Sauval (1998) photospheric abundances. The emissivity curves are plotted in Figure 2. The Si III line, typical of transition region plasma, is fairly weak and strongly contaminated by free-free emission and instrumental scattered light. It is therefore not considered in this work.

The spectra were acquired from an off limb section of the corona that was imaged through the 4×300 arcsec² SUMER slit. The slit was oriented in the north-south direction. During the observations, the solar diameter as seen from *SOHO* was $964''$ and the slit center was located at $W1030''$, $N300''$, i.e., at $1.10R_{\odot}$. The slit was nearly perpendicular to the radius vector with the center at a height of 7×10^4 km above the limb. The observation times, the number of spectra obtained with each sequence during the study, and the sequence of spectral lines used, are listed in Table 3.

Figure 3 displays images recorded in the Fe XIX line (upper panel), the Ca X line or the Ca XIII line (middle panel) and the free-free continuum (lower panel) at 1115 \AA during the 38 hour period considered in the present work. The Ca XIII image is displayed in the center section, between 05:46 UT and 18:22 UT April 24, 2003, and the Ca X line is shown on both ends. The images of Figure 3 were constructed as follows. First, for individual

spectra we fitted Gaussian profiles to spectral line features after removing the background (continuum), and obtained integrated line fluxes as a function of position along the slit. The free-free emission was obtained from a narrow part of the spectrum devoid of lines and later normalized to its value for a 1\AA wide wavelength band. Second, we stacked the individual spectrum integrated fluxes one next to the other such that the abscissa in Figure 3 represents time and the ordinate represents direction along the slit. To a large extent the resultant images are analogous to streak camera images often obtained in the laboratory to record time varying events.

Figure 3 shows the presence of several enhancements of Fe XIX and the free-free continuum. The bright SUMER events correlate fairly nicely in time with the presence of *GOES* flares. Figures 4a, 4b, 4c and 4d display for each of the recorded flares the line and continuum fluxes measured in four sections of Figure 3. The fluxes were derived from the average of 11 pixels (along the slit) centered on the horizontal white lines in Figure 3. Figures 4a to 4d also display Doppler shifts and widths vs. time of the Fe XIX, Ca X, or Ca XIII lines. In order to determine Doppler shifts from an Fe XIX wavelength measurement two pieces of information are required: knowledge of the rest wavelength of the Fe XIX line, which is well-established, and one or more nearby reference line wavelengths known not to be shifted. The Doppler shifts in Figure 4 are determined relative to wavelengths of reference lines emitted by chromospheric disk plasmas. The reference line spectra are scattered into the spectrometer slit by imperfections on the SUMER front telescope mirror and thus can be observed in spectra obtained above the limb. The chromospheric reference lines are emitted by ions of low degrees of ionization that are assumed to be at or very close

to their rest wavelengths. These lines are available for measurement from spectra recorded occasionally using the entire window of the detector.

The images in Figure 3 and the plots in Figures 4 show that times of abrupt increases in the Fe XIX flux correspond to times of decreasing Ca X flux at the identical spatial locations, although the decreases begin about ten minutes earlier than the Fe XIX increases. In addition the Fe XIX line shifts and widths indicate that during the abrupt increase in flux the flaring plasmas within the slit field-of-view experienced damped oscillations and non-thermal velocity increases. This is clearly the case in the events marked (b) and (c). In the (d) event moderate oscillations were observed using the Ca XIII line. The same is also seen in the fairly faint event near the end of the image of Figure 3 that is not discussed in this paper. Notice that prior to the flare eruptions the Ca X emission appears to be approximately uniform along the slit (ordinate) while the flux (flux) distribution (middle panel of Figure 3) of the Ca XIII line is concentrated in a few bands, most likely associated with post flare loops.

3. RESULTS

3.1 *Plasma Properties Based on GOES Observations*

In a statistical analysis of several hundred flares recorded by the Bent Crystal Spectrometer (BCS) on *Yohkoh*, Feldman et al. (1996) derived relationships among X-ray classes of flares (as defined by the *GOES* 1-8 Å detectors), emission measures, and temperatures at times corresponding to flare maximum. Using these relations, depicted in Figures 6 and 8 of Feldman et al. (1996), we estimated the total emission measures at peak

flux and peak temperatures of the flares under discussion. The derived values are given in Table 1, columns 3 and 4. The uncertainty in determining emission measure from *GOES* classes is $\pm 1/2$ order of magnitude and the uncertainty in determining the peak temperature from the *GOES* class is on the order of $\pm 3 \times 10^6$ K.

3.2 Emission Measures Based on SUMER Observations

The flux F (photons $\text{cm}^{-2} \text{s}^{-1}$) of an optically thin line or of free-free emission in 1 \AA intervals at a distance D can be written as,

$$F = \frac{A \times G(T_e, n_e)}{4\pi D^2} \langle EM \rangle \quad (1)$$

where A is the ratio between the abundance of the element in the corona and the photosphere (also referred to as the FIP bias), and $G(T_e, n_e)$ is the emissivity calculated with photospheric abundances, and includes atomic and temperature dependent quantities. The emission measure $\langle EM \rangle$ is defined as,

$$\langle EM \rangle = \int_V n_e^2 dV = \langle n_e^2 V \rangle \quad (2)$$

where n_e is the electron density and V the emitting volume. There is a proportionality factor is 0.8, not shown in equations (1) or (2), corresponding to the proton to electron ratio, but it is included in $G(T_e, n_e)$ in Equation (1). The emissivity for the lines and free-free continuum used herein are plotted in Figure 2. The properties of the free-free continuum in the Fe XIX wavelength range are discussed in detail in Feldman et al. (2003). The temperature in Figure

2 is plotted such that it decreases in values from left to right in order to match roughly the shape of the emissivity curves with actual flare line fluxes as they vary with time.

Flaring plasmas consist, primarily, of fully ionized H and He atoms. The Ca X line, formed at temperatures of $6 \times 10^5 \leq T_e \leq 2 \times 10^6$ K, can be used as a tracer indicating the presence of coronal plasma. The Fe XIX line formed at temperatures of $4 \times 10^6 \leq T_e \leq 1.4 \times 10^7$ K is a tracer indicating the presence of flaring plasmas, and the Ca XIII line formed at temperatures of $1.9 \times 10^6 \leq T_e \leq 5 \times 10^6$ K is a tracer for plasmas associated with the high temperature component of active regions or with post-flare loop plasmas. When flux changes in coronal or flaring lines occur at the same time and in the same place, the implication is that the emission measures of coronal and flaring plasmas also correspondingly change. Assuming a uniform distribution of plasma along the line-of-sight, the emission measure of the plasma that appeared or disappeared can be written as,

$$\langle EM \rangle = n_e \times (n_e V) \quad (3)$$

and is a product of the electron density multiplied by a quantity proportional to the amount of emitting plasma.

Free-free continuum emission in the solar upper atmosphere is produced primarily by the interactions between electrons and nuclei of hydrogen and helium. The emissivity in the SUMER range of the free-free continuum changes by only a factor of 2 between 1×10^5 K and 1×10^7 K (Figure 2). Because of this weak temperature dependence, it is a reliable indicator of transition region, coronal, and flaring plasma emission measures. Using fluxes

plotted in Figures 4b, 4c and 4d, the emission measure of a volume defined by a spatial pixel area of $4 \times 1 \text{ arcsec}^2$, and a line-of-sight length L , can be determined from Equation (1) as

$$\langle EM \rangle = 4\pi D^2 \frac{F}{G(n_e, T_e) \times A} \quad (4)$$

where in the case of the free-free continuum, $A=1$.

The emission measures per spatial pixel at peak flux for the flares designated as (b), (c) and (d), derived from the free-free continuum, are given in Table 1, column 8. The free-free continuum associated with the flares was calculated using the plots in Figures 4b to 4d, after removing the free-free flux before the onset of the events. The total emission measure along the SUMER slit is given in Table 1, column 9. This has been obtained by summing the free-free emission in all pixels along the slit where Fe XIX is enhanced. By comparing the emission measures from *GOES* and the emission measure along the SUMER slit we conclude that only $\sim 1\%$ of the total emission measure in each observed flare was recorded by SUMER.

This conclusion is consistent with EIT images taken during the SUMER flare observations. These images indicate quite clearly that the main brightening of the flare, i.e., the location of most of the flare emission measure, occurred considerably below the height of the SUMER slit. These observations are consistent with *Yohkoh* SXT observations that show that flares seldom reach heights of 70,000 km unless the flares are long duration events. Examples of images of intense flares that last tens of minutes and a long duration (tens of hours) flare that occurred above the limb are given in Feldman (1996).

Before continuing with the analysis of the results it is important to consider the following. The observed decrease in the coronal emission measure indicated by the decrease in the Ca X and Ca XIII line fluxes may be the result of the following:

- 1) A decrease in coronal plasma electron density (n_e), which may be a result of a sudden expansion of the plasma volume.
- 2) A decrease in the amount of coronal plasma ($n_e V$) along the line-of-sight, which can occur either because the plasma was suddenly heated from its coronal temperature ($T_e \leq 2 \times 10^6$ K) to flare temperatures ($T_e \geq 4 \times 10^6$ K), or as a result of plasma moving out of the field-of-view.
- 3) A combination of the cases described in (1) and (2).

No significant net motions along the line-of-sight or line broadening is present in the Ca X and Ca XIII lines displayed in Figures 4b, 4c, and 4d. This is consistent with in situ heating of coronal plasma to flare temperatures, but because the measured Doppler motions are limited to the line-of-sight component of the total motion, the possibility of radial motions moving plasma out of the SUMER field-of-view cannot be ruled out. (However, see the discussion of bulk motions in Section 3.5). In the in situ heating picture the Ca X line would have to start decreasing in flux prior to any observed increase in the flux of the Fe XIX flare line. As mentioned, there is about a 10 minute delay between the start of the decrease of Ca X line flux and the appearance of the Fe XIX line. The actual time difference would be explained in this scenario as due to the time necessary to heat the

plasma to Fe XIX emitting temperatures and produce sufficient emission measure for the Fe XIX line to be detected.

In analogy to the coronal plasma, the sudden increase of flaring emission measure could be due to the following:

- 1) An increase in the amount of flare plasma ($n_e V$) along the line-of-sight, which could occur either because colder plasma along the line-of-sight ($T_e \leq 2 \times 10^6$ K) was heated to flare temperatures ($T_e \geq 4 \times 10^6$ K), or because plasma at flaring temperatures moved into the field-of-view.
- 2) An increase in the flare electron density (n_e), perhaps as a result of a compression.
- 3) A combination of the cases described in (1) and (2).

In Section 3.5, we discuss net Doppler shifts detected in the Fe XIX line and conclude that net motions, if present, most likely did not exceed several tens of km s^{-1} , a velocity not sufficiently large to move the plasma on time into the field of view. If this conclusion is valid, it is quite possible that the increase in the flaring emission measure is due to coronal plasma heated in situ to flare temperatures. An increase in the electron density could also occur concurrently with the heating process. In this scenario, electron density changes in the coronal plasmas during the heating process can be derived from the relationship

$$\frac{n_e(\text{flare})}{n_e(\text{corona})} = \frac{EM(\text{flare})}{EM(\text{corona})} \quad (5)$$

where we assume that the initial and final number of particles ($n_e V$) in the coronal and flare plasmas are the same. Another implicit assumption is that the coronal and flare emission measures are representative of the same plasma, which may not be strictly true because the derived coronal and flare emission measures do not refer to the same temperature ranges. Since heating of plasma from coronal to flare temperatures must take a certain amount of time, the appearance of flare plasma might only be detectable a substantial time after the coronal plasma begins disappearing as indicated by decreasing Ca X line fluxes.

3.3 *Electron Densities Based on SUMER Observations*

To estimate the electron density we assume that the length of the plasma along the line-of-sight was $L=1 \times 10^3$ km and the volume filling factor was $f=1$. Using these assumptions and the earlier obtained emission measure values, the flaring electron density during peak emission was derived from the relationship

$$n_e = \sqrt{\frac{\langle EM \rangle}{f \times V}} \quad \text{cm}^{-3} \quad . \quad (6)$$

The derived electron densities (log values) are listed in Table 1, column 10. We believe that these values are only lower limits, since the filling factors are most likely much smaller than unity. It is difficult to imagine that L is much larger than 1×10^3 km because even for the brightest flares observed by *Yohkoh* loop diameters are not larger than 1×10^4 km (Feldman et al. 1994).

3.4 *Electron Temperature and Elemental Abundances From SUMER Observations*

The electron temperature of the flaring plasmas can be determined from the flux ratio of the Fe XIX line to the free-free continuum provided that the iron elemental abundance in the plasma is known. However, iron is a low-FIP element and because of the FIP effect its abundance could be larger than its photospheric value. In the current study we do not have a sufficient number of spectral lines to derive the iron abundance in each of the observed flaring plasmas. Nevertheless, we can derive the iron abundance late in the decay phase of flares (c) and (d). We can do this because at these times the diagnostic lines Fe XIX, Fe XVII, Ca XIII, as well as the free-free continuum were observed simultaneously.

Using the emissivity curves of Figure 2 and the Fe XIX/Ca XIII, Fe XIX/Fe XVII and Fe XVII/Ca XIII flux ratios we determined for example that the plasma temperature of flare (d) at 18:00 UT, April 24 was 4.0×10^6 K. Given the plasma temperature, and the Fe XIX, Fe XVII, and Ca XIII line to free-free flux ratios, we find that the flaring plasma was FIP enriched by a factor of 8-10. (Fe and Ca are both low FIP elements.) In a similar analysis we derived a FIP bias of 8 late in the decay phase (07:00 UT) of flare (c). A FIP bias of 8-10 is typical of plasmas in active regions that are at least 7 days old (Widing & Feldman 2001; Feldman & Widing 2003; Young & Mason 1998). As mentioned in Section 2.0, images of the active region above which the flares erupted, recorded by MDI and EIT on *SOHO*, indicate that it was at least two weeks old. Also, the diverging open field line morphology of the coronal structures that are clearly visible on EIT images when the region was near disk center is typical for regions with unusually large abundance enrichments of low-FIP elements.

By adopting a FIP bias of 8 for flares (b) and (c) and a FIP bias of 9 for flare (d), we derived the plasma temperatures for the times of peak Fe XIX emission for these flares. The derived temperatures are listed in Table 1, column 7. Notice that the derived temperatures for flares (c) and (d) are significantly lower than those estimated from the *GOES* data. For the flare that erupted at ~5:30 UT, April 24, about 40 minute after flare (c), the SUMER derived temperature is even lower. We partly attribute this discrepancy to the fact that the contribution to the *GOES* X-ray flux, from which the temperature was determined, came from two flares, the limb flare observed by SUMER and a disk flare detected by H α observations. Also, *GOES* temperatures should be systematically higher than SUMER Fe XIX temperatures because *GOES* is sensitive to iron ionized substantially more than Fe XIX. Nevertheless, the derived Fe XIX temperatures are much larger than those present in coronal or post flare loop plasmas.

Using the limited number of lines observed during the flare campaign, we could not determine the coronal plasma temperature from the Ca X line alone. Therefore, in the following we resort to knowledge accumulated from other SUMER observations. Temperatures of coronal plasmas at heights of 1.05-1.3 R_{\odot} are expected to be in the $1.3 \times 10^6 \leq T_e \leq 2 \times 10^6$ K range (For examples of coronal plasmas properties high above the solar limb see Feldman et al. 1999, Landi & Feldman 2003). Given this temperature range and assuming a coronal temperature of $T_e = 1.6 \times 10^6$ K, the amount of coronal emission measure depleted during the flare onset can be determined with an uncertainty of $\pm 50\%$. Using the Ca X fluxes in Figures 4a, 4b, and 4c, at times when the Fe XIX fluxes peaked, and the emissivity curve in Figure 2, the depleted coronal emission measure values listed in

Table 1, column 11 were derived. In a similar way we assumed that the temperature of the plasma emitting the Ca XIII line prior to the eruption of flare (d) was $2 \times 10^6 \leq T_e \leq 3.5 \times 10^6$ K. Using the decrease in the Ca XIII flux during the onset of the flare plotted in Figure 4d and assuming a plasma temperature of 2.6×10^6 K, we determined the missing emission measure with an uncertainty of $\pm 50\%$. The derived value is listed in Table 1, column 12. Most of the uncertainties in the emission measure are due to uncertainties in the atomic data and in the temperature.

By substituting in Equation (5) the values of the flaring and coronal emission measures we conclude, depending on the adopted Ca X formation temperature (1.3 or 2×10^6 K), that the electron density increased by factors of 25 and 250 in flares (b) and (c) respectively. This conclusion assumes that the number of particles in the missing coronal plasma is the same as the number of particles in the Fe XIX flare plasma. From a comparison of the emission measures obtained from the Ca XIII line and the free-free continuum associated with the flare (d), it appears that the factor by which the electron density increased was 13. The values we derive are much larger than the uncertainties of the present analysis (see Table 1).

3.5 Shifts and Widths of the Fe XIX Line

Determining the net motions of plasma from Doppler measurements alone is strictly speaking not possible unless imaging information is also available. In this work the only available bulk motion data are line-of-sight motions nearly perpendicular to the solar radial direction. Motions perpendicular to the line-of-sight cannot be measured because imaging

information is not available. If motion occurs in the solar radial direction precisely at right angles to the line-of-sight, no line-of-sight velocity will be measured no matter how large the velocity in the solar radial direction.

However, a rough estimate of net motions can be inferred if a large number of limb events are observed. In this situation one expects that motions will occur along tracks distributed around the direction perpendicular to the SUMER line of sight, i.e., an event might occur at E80 or W80 and not exactly at E90 or W90. In this case the angle between the solar radial direction and the line-of-sight is somewhat less or greater than 90 degrees, and the solar radial motion will produce measurable motion along the line-of-sight. We consider that a spread of angles within a 20 degree cone about the 90 degree direction is a reasonable expectation for a large sample of limb events. For example, an event at a height H_0 above the limb and a solar radial velocity v_0 which erupts in an active region located at E70 or W70 will have the projected height of $H' = H_0 \sin 70 = 0.94 H_0$, however, the net velocity detected by the observer would be substantial ($v = v_0 \cos 70 = 0.34 v_0$).

Wang et al. (2003) reported the observation above the limb of 54 flares. Although they discuss oscillations and not net velocities in the events they measured, it is clear from the figures presented in their paper that little or no line-of-sight Doppler shifts of the Fe XIX rest wavelength exist for their events. From such a sample of flares, one might have expected to find at least some events with substantial rest wavelength shifts if there were substantial motions along the solar radial direction. Wang et al. (2003) do not interpret any of their results in terms of an outflow of plasma in solar radial directions. Their results, coupled with the fact that our Fe XIX wavelengths indicate at most only a few km s^{-1} line-

of-sight motions, suggest that the solar radial motions, if they exist at all, are mostly likely also only in the range of tens of km s^{-1} .

The slit pointing of the observations was above the limb. Assuming that any net plasma motions are in a solar radial direction, the velocity along the line-of-sight, v_s , is the product of the actual velocity, v_0 , and the cosine of the angle between the solar radial motion and the line-of-sight, i.e., $v_s = v_0 \cos\theta$. Using information provided in the Solar Geophysical Data Comprehensive Reports, we estimate that flare (b) occurred at N17:W82, flare (c) at N17:W86, and flare (d) at N17:W92. Assuming that these locations are good indicators of the radial direction of the motions, line-of-sight velocities of $v_s = 5 \text{ km s}^{-1}$ from regions N17, W82 and N17, W86 correspond to a v_0 of 36 and 72 km s^{-1} respectively. This result is in agreement with the BCS/*Yohkoh* 3.2 Å Ca XIX line measurements where it was determined that during the rise phase of 219 disk flares the average radial velocity was 58 km s^{-1} (Mariska, Doschek & Bentley 1993).

Despite all these hints, the present data set does not allow us to rule out completely the present of large radial motions. It is clearly desirable to observe flares by a spectrometer and with an imaging spectrometer so that the motions perpendicular to the line-of-sight can be directly observed. This will require new generation spectral/imaging instrumentation.

As is the case for the events discussed by Wang et al. (2003), at flare onset the plasma represented by the Fe XIX line underwent several damped oscillations with a period of 10-15 minutes and initial amplitudes of $A(0) = 50\text{-}100 \text{ km s}^{-1}$. In spite of the clear oscillatory motion little or no net mass motions along the line-of-sight are present. The

wavelength of the Ca X line that represents the remaining coronal plasmas shows no oscillations or any net plasma motions larger than 2 km s^{-1} . The wavelength of the Ca XIII line shows low amplitude oscillations ($A(0) \leq 7 \text{ km s}^{-1}$) at flare onset (flare (d)).

The full width at half maximum (FWHM) of a spectral line can be expressed as

$$FWHM = \left(\Delta\lambda_{\text{ins}}^2 + \frac{\lambda_0^2}{c^2} 4 \ln 2 \left[\frac{2kT_i}{M} + \xi^2 \right] \right)^{1/2} \quad (7)$$

where $\Delta\lambda_{\text{ins}}$ is the width contribution due to instrumental factors associated with the 4 arcsec wide entrance slit, λ_0 is the rest wavelength of the line under consideration, c the speed of light, T_i is the ion temperature, and ξ is the non-thermal mass motion of the emitting ions. Assuming that $T_i = T_e$ (T_e the electron temperature), the non-thermal velocity can be evaluated once the instrumental width is removed. Line widths in Figure 4 are displayed as FWHM in Angstrom units. At flare onset when temperatures are on the order of $8 \times 10^6 \text{ K}$, a FWHM of 0.6 \AA corresponds to 79 km s^{-1} , 0.5 \AA corresponds to 58 km s^{-1} and 0.4 \AA to 35 km s^{-1} . Late in the flare when the temperature is $4 \times 10^6 \text{ K}$, 0.35 \AA line width corresponds to 35 km s^{-1} . From the plots in Figures 4 one sees that at flare onset non-thermal mass motions were between 50 and 100 km s^{-1} and at later times they decrease to values approaching 35 km s^{-1} .

4. SUMMARY AND DISCUSSION

In this paper we have derived physical properties of ambient coronal and flaring plasmas during a 38 hour period. The plasma properties were deduced from SUMER

observations in the Ca X, Ca XIII, the Fe XIX lines and in the free-free continuum. The observations were obtained with the slit pointed 7×10^4 km above the limb at times when a number of flares erupted in an old active region, enabling physical conditions to be determined in coronal and flaring plasma prior, during, and after the flare events. We used the Fe XIX forbidden line and free-free continuum as representative tracers of flare plasmas ($\sim 1 \times 10^7$ K) and the Ca lines as representative tracers of coronal plasmas ($\sim 1 \times 10^6$ K) in which the flare emission is imbedded. The main results are summarized below:

- 1) Emission measures of the flares were derived from *GOES* observations. Using a 4×300 arcsec² entrance slit, which imaged plasmas at $\sim 7 \times 10^4$ km above the limb, SUMER detected $\sim 1\%$ of the total flare emission measure, an indication that only a small fraction of the flare plasmas reached the height of 7×10^4 km.
- 2) Prior to the flares the flux of the coronal plasma ($T_e \sim 1.6 \times 10^6$ K) along the SUMER slit appears to be fairly uniform. However, about ten minutes before the first appearance of the Fe XIX flare line, the coronal line flux weakens in the location where the flare plasma later appears.
- 3) No significant Doppler shifts and sudden line broadening are observed in the Ca X coronal line.
- 4) At flare onset the plasma represented by the Fe XIX flare line underwent a sequence of damped oscillations around the rest wavelength with a period of 10-15 minutes and initial amplitude of $A(0) = 50-100$ km s⁻¹. In spite of

this oscillation, only little or no net mass motions are observed along the line-of-sight.

- 5) The elemental abundances of low FIP calcium and iron are enhanced by a factor of 8-10 relative to their abundance in the photosphere. This is significantly larger than any enrichment previously observed in the chromosphere, and strongly indicates that the flare plasma originated from coronal, and not fresh chromospheric, plasma.
- 6) From a comparison of the SUMER coronal and flare emission measures, and from the assumption that the flare plasma was heated coronal plasma, i.e., that the number of particles in the coronal and flare plasma was the same, we determined that the flare plasma underwent an approximately two orders of magnitude increase in electron density relative to the coronal electron density. Assuming a coronal electron density at a height of 7×10^4 km of $\sim 1 \times 10^8 \text{ cm}^{-3}$ (Landi & Feldman 2003), and a filling factor of 1, the flare electron densities at peak brightness are $1 \times 10^{10} \text{ cm}^{-3}$, in rough agreement with independent estimates from the free-free emission. These results are consistent with typical compact flare densities obtained from *Skylab* observations (e.g., Moore et al. 1980).

The heating, high electron density, the unusually high FIP bias, and the absence of net motions determined from the present work are supportive of an in situ heating scenario for the flare plasma observed by SUMER. Because of the large enhancement of low FIP

elements, it is unlikely that the heated plasma is freshly evaporated chromospheric plasma. In the in situ heating picture the delay between onset of decreasing Ca line flux and increasing Fe XIX flux would be due to the time necessary to heat the plasma to Fe XIX emitting temperatures as well as provide sufficient emission measure for the Fe XIX line to be detected. The strongest support for in situ heating is the large FIP enhancement of the flare plasma, which is difficult to understand if the flare plasma is freshly evaporated chromospheric plasma. The absence of very large motions is also supportive of in situ heating, but in this case the support is somewhat weaker because of the difficulty in estimating the actual angle of the motions relative to normal. In fact, movies constructed in streak mode by Harry Warren (private communication) using EIT data from the Fe XII channel show radial outflow motions over the entire region of the SUMER observations, but it is not clear what the Fe XXIV/Fe XII emission ratio is in the EIT data.

One may argue that the 10^6 K coronal plasma disappeared from the slit field-of-view as a result of an influx of 10^7 K flare plasma that displaced the coronal plasma. However, from the observed flare and coronal plasma emission measures and densities, we know that the flare volume occupied by the flare plasma appearing in the field-of-view is much less than the volume occupied by the disappearing coronal plasma. It seems difficult to understand how the presence of a small volume of flare plasma would require the disappearance of a much larger volume of coronal plasma.

If the flare plasma observed by SUMER is due to in situ heating, the high flare densities are suggestive of a compressive mechanism in the corona because typical background coronal densities are at least an order of magnitude less than the flare densities.

The Alfvén & Carlqvist (1967) current interruption model may provide the basis for such a mechanism. The model is based on the idea that hot plasma can be generated by a sudden discharge of an electric current into a loop already filled with plasma at a coronal density and temperature. One scenario is that the sudden discharge of the current along the magnetic lines of force creates an azimuthal magnetic field B_θ , which exerts pressure on the coronal plasma and consequently compresses and heats it. In this picture the line broadening we observe might be related to the compression. Also the initial impulsive release of electric current might generate a mechanical shock that causes the loop to oscillate.

To get an estimate of the magnitude of the azimuthal magnetic field B_θ that could produce the electron densities seen during flare maximum we assume that the flare plasma was confined to a single loop and that the plasma in the coronal loop was compressed to a density of n_{ep} . We further assume the presence of an axial magnetic field B_z along the loop. A relationship between the magnetic fields and the electron density can be estimated from the equation

$$\frac{B_\theta^2}{8\pi} \geq 2nkT_{ep} + \frac{B_z^2}{8\pi} \quad (8),$$

where k is the Boltzmann constant and T_{ep} is the temperature at the peak of the flare emission. Using a temperature of $T_{ep}=8 \times 10^6$ K and $n=1 \times 10^{10} \text{ cm}^{-3}$, which may turn out to be a lower limit, we obtain

$$B_\theta \geq \sqrt{5.5 \times 10^2 + B_z^2} \quad . \quad (9)$$

Assuming an axial field of $B_z=50$ gauss we derive an azimuthal field during peak compression of $B_\theta \geq 55$ gauss. For a similar assessment relating to a much larger flare that was analyzed using X-ray spectra see Feldman et al. (1980).

Whatever the explanation of the SUMER flare results, it is clear that high spectral and spatial resolution spectroscopic data for flares provide important diagnostics that complement imaging observations. Hopefully the upcoming *Solar-B* mission (launch 2006) will last long enough for the Extreme-ultraviolet Imaging Spectrometer (EIS) on *Solar-B* to observe many flares over a much larger spatial region than is possible with SUMER.

ACKNOWLEDGEMENTS

We thank Drs. Jim Klimchuk, Martin Laming, John Seely, Szymon Suckewer, Harry Warren, and Ken Widing for helpful discussions. We also thank the referee for helping us clarify points in the original version. The work reported in this paper was supported by ONR/NRL 6.1 funds. EL acknowledges support from a NASA Living With a Star & SR&T grants. The SUMER project is financially supported by DLR, CNES, NASA, and ESA PRODEX program (Swiss contribution). SUMER is part of *SOHO*, the *Solar and Heliospheric Observatory* of ESA and NASA.

REFERENCES

- Alfvén, H., & Carlqvist, P. 1967, *Solar Phys.*, 1, 220
- Athay, R.G. 1994, *ApJ*, 423, 516
- Delaboudinière, J.-P., et al. 1995, *Solar Phys.*, 162, 291
- Dere, K.P., Landi, E., Young, P.R. & Del Zanna, G. 2001, *ApJS*, 134, 331
- Doschek et al. 1986, *Energetic Phenomena on the Sun, Ch. 4, "Chromospheric Explosions"*,
NASA Conf. Publ. 2439
- Doschek, G.A., Feldman, U., Kreplin, R.W., & Cohen, L. 1980, *ApJ*, 239, 725
- Feldman, U. 1996, *Phys. Plasmas*, 3, 3203
- Feldman, U., Doschek, G.A., & Kreplin, R.W. 1980, *ApJ*, 238, 365
- Feldman, U., Doschek, G.A., Kreplin, R.W., & Mariska, J.T. 1980, 241, 1175
- Feldman, U., Seely, J.F., Doschek, G.A., Strong, K.T., Acton, L.W., Uchida, Y., & Tsuneta,
S. 1994, *ApJ*, 424, 444
- Feldman, U., Doschek, G.A., Behring, W.E., and Phillips, K.J.H. 1996, *ApJ*, 460, 1034
- Feldman, U., Doschek, G.A., Schühle, U., and Wilhelm, K. 1999, *ApJ*, 518, 500
- Feldman, U. & Laming, J.M. 2000, *Physica Scripta*, 61, 222
- Feldman, U., Landi, E., Doschek, G.A., Dammasch, I. and Curdt, W. 2003, *ApJ*, 593, 1226
- Feldman, U. & Widing, K.G. 2003, *Space Sci. Rev.*, 107, 665
- Feldman, U. Widing, K.G., & Lund P.A. 1990, *ApJ Letters*, 364, L21
- Grevesse, N., & Sauval, A.J. 1998, *Space Sci. Rev.*, 85, 161
- Landi, E., & Feldman, U. 2003, *ApJ*, 592, 607
- Li, P., Emslie, A.G., & Mariska, J.T. 1989, *ApJ*, 341, 1075

Mariska, J.T., Doschek, G.A. & Bentley, R.D. 1993, ApJ, 419, 418

Mazzotta, P., Mazzitelli, G., Colafrancesco, S. & Vittorio, G. 1998, A&A, 133, 403

Moore, R., et al. 1980 “*Solar Flares: A monograph from Skylab Solar Workshop*”

McKenzie, D.L. & Feldman, U. 1992, ApJ, 389, 764 *IP*’ Colorado Associated University
Press, Edited by Peter Sturrock, page 388

Scherrer, P.H., et al. 1995, Solar Phys., 162, 129

Wang, T.J., Solanki, S.K., Curdt, W., Innes, D.E., Dammasch, I.E. & Kleim, B. 2003, A&A,
406, 1105

Widing, K.G., & Feldman, U. 1989, ApJ, 344, 1046

Widing, K.G., & Feldman, U. 1993, ApJ, 416, 392

Widing, K.G., & Feldman, U. 2001, ApJ, 555, 426

Wilhelm, K. et al. 1995, Solar Phys., 162, 189

Young, P.R., Del Zanna, G., Landi, E., Dere, K.P., Mason, H.E., Landini, M. 2003, ApJS,
144, 135

Young, P.R., & Mason, H.E. 1998, Space Sci. Rev., 85, 315

TABLE 1 - Information and Plasma Properties of X-ray Class \geq C2 Flares Recorded by *GOES* and SUMER Between 14:00 UT

April 23 and 04:00 April 25, 2003

From <i>GOES</i> 12											
From <i>GOES</i> 12 (Estimated at Flare Max)				H α Location	From SUMER .						
Onset Time ¹ (UT)	<i>GOES</i> Class	EM ²	T _e (K) ²		Fe XIX Onset Time	Fe XIX/ FF at Peak T _e (K)	From Free-free Log EM ³ per Spatial Pixel (cm ⁻³) Log EM ⁴ Along the Slit (cm ⁻³) Log n _e (cm ⁻³)			From Ca X Log EM ³ Depletion per Spatial Pixel (cm ⁻³)	From Ca XIII Log EM ³ Depletion per Pixel (cm ⁻³)
April 23											
15:30	M2	48.3-49.3	2.0x10 ⁷	N17, W78							
21:30 (b)	B8	47.2-48.2	1.2x10 ⁷	None	21:30	4.9x10 ⁶	43.9±0.3	45.4	9.8	42.9±0.3	
April 24											
04:50 (c)	C7	48.0-49.0	1.6x10 ⁷	None	04:54	8.0x10 ⁶	44.7±0.15	46.3	10.2	42.5±0.4	
05:30	C5	47.8-48.8	1.6x10 ⁷	S15, E08	05:40	5.3x10 ⁶	44.7	46.3	10.2		
12:50	M3			N21, W39							
15:45 (d)	C8	48.0-49.0	1.7x10 ⁷	None	15:45	9.0x10 ⁶	44.5±0.1	46.6	10.1		43.6±0.3

¹ The letters (b), (c) and (d) are the same as in Figure 1. We did not list the event marked (a) in Figure 1 in the table because it is quite weak. It was not detected by ground-based H α telescopes, and it is not clearly noticeable in Figure 3.

² From Figures 6 and 10 in Feldman et al (1996)

³ Emission measure per pixel at flare maximum derived from averaging 11 pixels centered on the horizontal white lines in Figure 3.

⁴ The emission measure obtained by summing the flare emission along the SUMER slit.

TABLE 2 - Observed Spectral Lines

Sequence Number	Ion	λ (Å)	Identification	T_{\max} (K)
1	Si III	1113.22	$3s3p\ ^3P_2-3s3d\ ^3D_3$	2×10^4
1	Ca X	1115.51/2	$3p\ ^2P_{3/2}-3s\ ^2S_{1/2}$	8×10^5
1	Fe XIX	1118.08	$2s^22p^4\ ^3P_1-2s^22p^4\ ^3P_2$	7.9×10^6
2	Fe XIX	1118.08	$2s^22p^4\ ^3P_1-2s^22p^4\ ^3P_2$	7.9×10^6
2	Ca XIII	1133.76	$2s^22p^4\ ^1D_2-2s^22p^4\ ^3P_2$	2.3×10^6
2	Fe XVII	1153.17	$2p^53s\ ^3P_0-2p^53s\ ^3P_1$	5.0×10^6

TABLE 3 - The SUMER Spectra

Start Date (DD/MM/YY)	Start/ End Time (HHMM-HHMM)	Cadence (s)	No. of Spectra	Sequence Number ¹
23/04/03	14:30-23:59	49.5	671	1
24/04/03	00:00-05:41	49.5	400	1
24/04/03	05:46-18:22	49.5	801	2
24/04/03	18:26-23:59	49.5	396	1
25/04/03	00:00-04:32	49.5	323	1

¹ The sequence number is given in Table 2

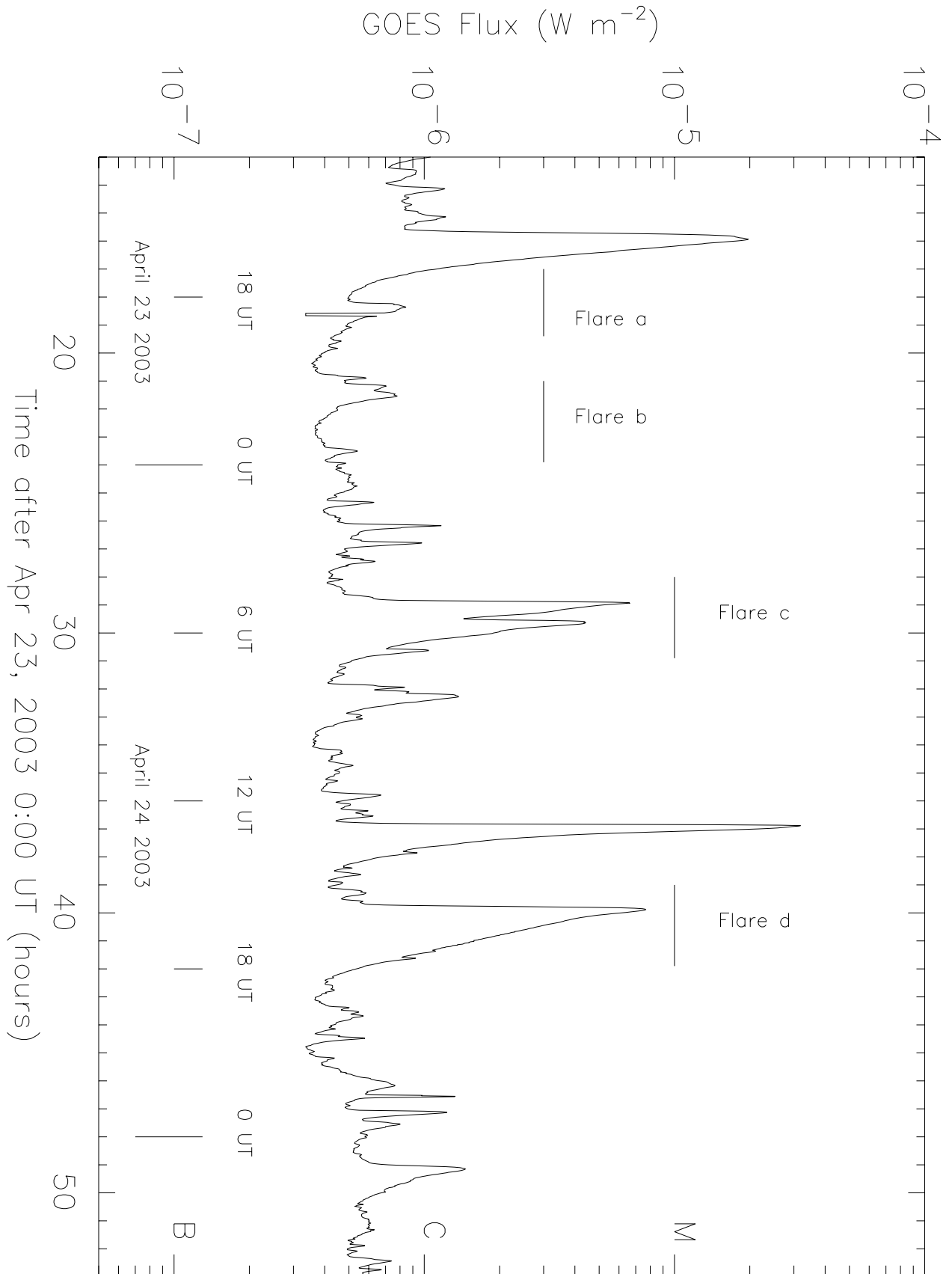
FIGURE CAPTIONS

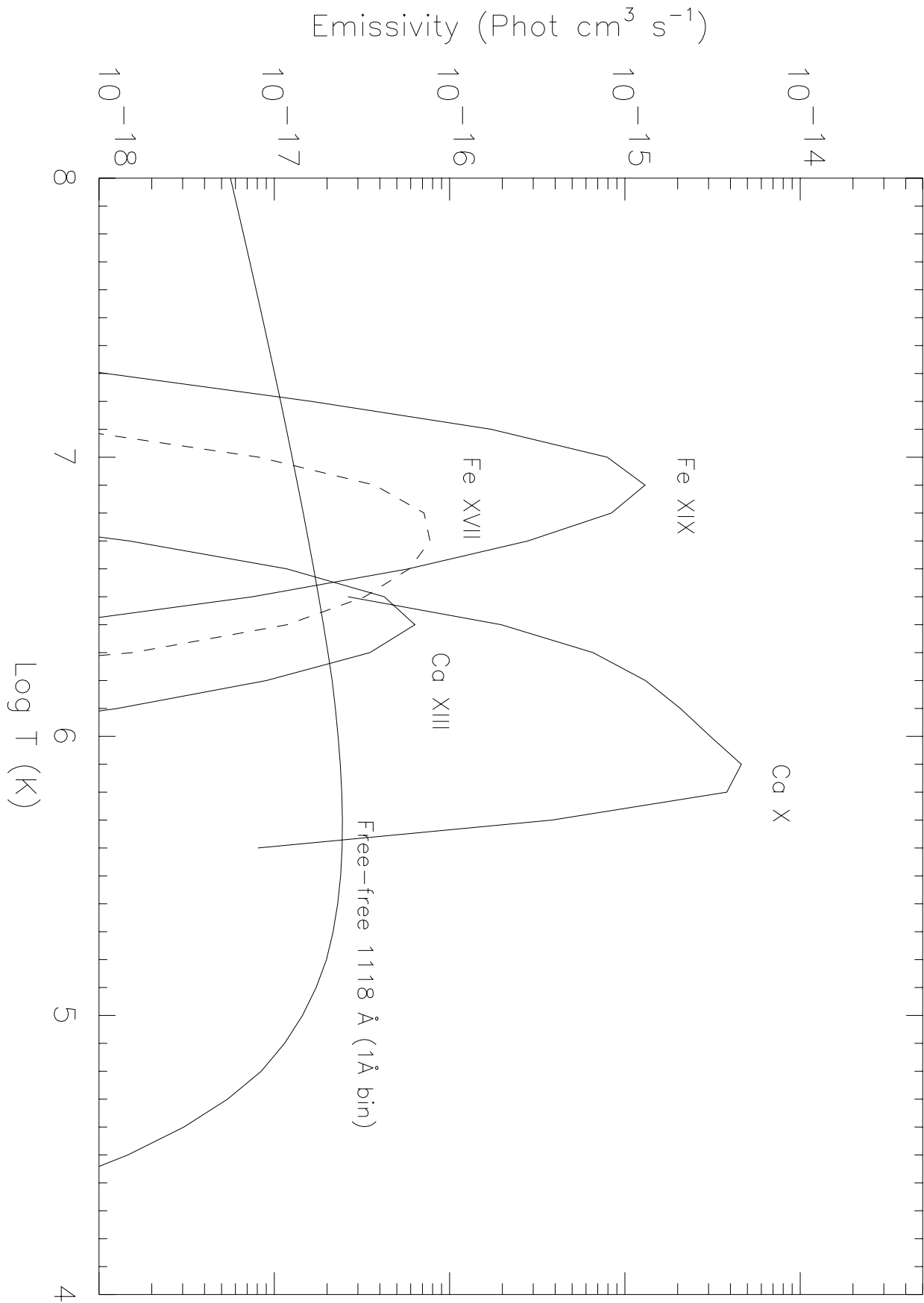
Figure 1 - Time sequence of *GOES* 12 X-ray flux in the 1-8 Å band. The flares considered in the present work are marked as Flare a, Flare b, Flare c and Flare d.

Figure 2 - Emissivity curves $G(T)$ for Fe XIX 1118 Å, Fe XVII 1153 Å, Ca XIII 1133 Å, and Ca X 557 Å as a function of temperature. The free-free continuum emissivity is integrated near 1118 Å.

Figure 3 - Fluxes vs. time in Fe XIX (top), Ca X, Ca XIII (center) and the free-free emission (bottom) for 38 hours between 14:30 UT, April 23 and 04:30 UT, April 25, 2003. The Ca XIII line is displayed in the center section, between 05:46 UT and 18:22 UT April 24, 2003, and the Ca X line is displayed on both ends.

Figure 4 - Figs. (a) & (b): Measurements of the Fe XIX line fluxes (top), line-of-sight speed (2nd from top), line widths (3rd from top) and the free-free flux (bottom left). Figs. (c) and (d): Fluxes of additional lines are also plotted. The fluxes are given in units of photons s⁻¹ cm⁻² arcsec⁻².





Spatial dimension

